




Cite this: DOI: 10.1039/c7lc00836h

 Received 7th August 2017,  
Accepted 23rd August 2017

DOI: 10.1039/c7lc00836h

rsc.li/loc

## Microfluidic bead trap as a visual bar for quantitative detection of oligonucleotides†

 Zichen Zhao,<sup>a</sup> Yuanye Bao,<sup>a</sup> Lok Ting Chu,<sup>b</sup> John Kin Lim Ho,<sup>a</sup>  
Ching-Chang Chieng<sup>a</sup> and Ting-Hsuan Chen \*<sup>abcd</sup>

We demonstrate a microfluidic bead trap capable of forming a dipstick-type bar visible to the naked eye for simple and quantitative detection of oligonucleotides. We use magnetic microparticles (MMPs) and polystyrene microparticles (PMPs) that are connected and form MMPs–targets–PMPs when target oligonucleotides are present, leaving free PMPs with a number inversely proportional to the amount of targets. Using a capillary flow-driven microfluidic circuitry consisting of a magnetic separator to remove the MMPs–targets–PMPs, the free PMPs can be trapped at the narrowing nozzle downstream, forming a visual bar quantifiable based on the length of PMP accumulation. Such a power-free and instrument-free platform enables a limit of detection at 13 fmol (0.65 nM in 20  $\mu$ l, S/N = 3) of oligonucleotides and is compatible with single-nucleotide polymorphisms and operation in a complex bio-fluid. Moreover, using DNAzyme as the target oligonucleotide that catalyzes a specific hydrolytic cleavage in the presence of lead ions, we demonstrate a model application that detects lead ions with a limit of detection of 12.2 nM (2.5  $\mu$ g l<sup>-1</sup>), providing quantitative and visual detection of lead contamination at resource-limited sites.

Detection of oligonucleotides provides immense potential for pathogen identification,<sup>1–4</sup> clinical diagnosis,<sup>2,5,6</sup> biomedical research,<sup>7,8</sup> and monitoring of metal ions.<sup>9–12</sup> In recent years, visual detection, as a simple, direct and rapid method, has been developed in many platforms, including AuNP-based colorimetric assays,<sup>13–15</sup> lateral flow strips,<sup>7,16</sup> magnetic barcode assays,<sup>17,18</sup> and magnetophoretic assays.<sup>19–21</sup> AuNP-based assays, in particular, have been widely applied to detect

oligonucleotides because of their rapid visual responses.<sup>13,14</sup> Typically, AuNPs are surface functionalized with single-strand oligonucleotide probes that can hybridize with target oligonucleotides in juxtaposition. As such, the presence of target oligonucleotides would induce the aggregation of AuNPs by forming a sandwich-type structure, *i.e.* AuNPs–targets–AuNPs, resulting in a change of bulk solution color from red to purple readable by visual inspection.<sup>22–24</sup> A similar principle was applied in the detection of ssDNA/RNA,<sup>24</sup> proteins<sup>25</sup> and metal ions.<sup>26,27</sup> To further simplify the operation, the scheme of the sandwiched structure evolved into lateral flow strips, in which gold nanoparticles carried by capillary flow are captured based on the hybridization between target oligonucleotides and probes immobilized on the substrates.<sup>16</sup> The accumulation of gold nanoparticles leads to a formation of a red bar visible to the naked eye. Similarly, to provide better sensitivity in visual detection, previously we developed a simple and effective visual detection of oligonucleotides based on Mie scattering and magnetophoretic effect,<sup>20</sup> allowing visual detection based on solution turbidity. However, although convenient, current platforms for visual detection are mostly limited to qualitative results (yes or no signal). For quantitative measurement, the visual signal needs to be converted into optical/fluorescence intensity measured using a lateral flow strip reader,<sup>16,28</sup> or spectral absorbance read using a UV-vis spectrometer.<sup>20,29</sup> As a result, cumbersome and bulky instruments and power supply are inevitable, which creates technical hurdles for detection and analysis in resource-limited settings.

Here we report a visual and quantitative detection of oligonucleotides based on a microfluidic bead trap (Fig. 1). MMPs and PMPs are surface functionalized with single-strand oligonucleotide probes such that the presence of MB155 targets would induce the formation of a sandwiched structure, MMPs–targets–PMPs. To visually count the number of free PMPs, which is inversely proportional to the amount of targets, we designed a microfluidic device with a bead trap. Carried by self-driven capillary flow, the MMPs–targets–PMPs

<sup>a</sup> Department of Mechanical and Biomedical Engineering, City University of Hong Kong, Hong Kong Special Administrative Region.  
E-mail: thchen@cityu.edu.hk

<sup>b</sup> School of Creative Media, City University of Hong Kong, Hong Kong Special Administrative Region

<sup>c</sup> Centre for Robotics and Automation, City University of Hong Kong, Hong Kong Special Administrative Region

<sup>d</sup> CityU Shenzhen Research Institute, Shenzhen, China

† Electronic supplementary information (ESI) available. See DOI: 10.1039/c7lc00836h

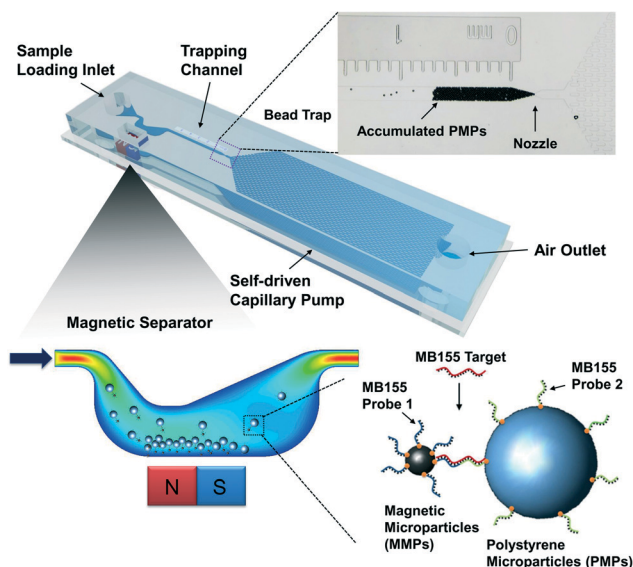


**Fig. 1** Schematics of the microfluidic bead trap forming a visual bar for detection of oligonucleotides. Carried by self-driven capillary flow, the aggregates of MMPs–targets–PMPs are first captured in the magnetic separator, allowing free PMPs to flow and be trapped by a nozzle downstream. As such, the PMPs accumulate with a length inversely proportional to the amount of target oligonucleotides readable to the naked eye, providing a visual and quantitative readout on a power-free and instrumental free platform.

are first captured in the magnetic separator, and the free PMPs can escape from the magnetic field and accumulate at the bead trap downstream. Thus, the accumulation of PMPs forms a visual bar with a length quantifiable by a ruler labeled above the trapping channel. This method allows for a limit of detection at 13 fmol (0.65 nM in 20  $\mu\text{l}$ , S/N = 3) for oligonucleotides and is capable of differentiating single-nucleotide polymorphisms and operation in a complex biofluid. Moreover, using DNAzyme as the target oligonucleotide that catalyzes a specific hydrolytic cleavage in the presence of lead ions, we demonstrate a model application that detects lead ions with a limit of detection of 12.2 nM (2.5  $\mu\text{g l}^{-1}$ ), which is below the maximum human exposure to drinking water, 48 nM (10  $\mu\text{g l}^{-1}$ ), according to the guideline of the World Health Organization, providing a simple approach achieving visual detection and direct quantification of lead contamination on a power-free and instrumental-free platform.

## Results and discussion

### Working principle

To detect a specific target oligonucleotide, *i.e.* MB155, two probes of biotinylated oligonucleotides (MB155 probe 1 and probe 2) were designed with a sequence complementary to MB155 in juxtaposition. MB155 probe 1 and probe 2 were respectively immobilized onto streptavidin-coated MMPs and PMPs *via* a biotin–streptavidin complex (lower-right in Fig. 1). As such, when the MB155 target is present, probe 1

and probe 2 will simultaneously hybridize with the MB155 target in juxtaposition, forming a sandwich-type aggregate, “MMPs–targets–PMPs” (for the detailed procedure and discussion of the hybridization process, see the ESI†). Notably, to prevent the inertial forces that may break the linkage between MMPs and PMPs, MMPs with a diameter of 0.36  $\mu\text{m}$  were selected, such that multiple MMPs can attach onto one PMP to disperse the force (Movie S1†). Thus, the number of free PMPs can be used as a reporter representing the amount of MB155 targets.

To automate PMP counting, we designed a microfluidic circuitry consisting of a sample loading inlet, a magnetic separator, a trapping channel with a ruler, a nozzle, a capillary pump and an air outlet (upper in Fig. 1). After rinsing, probe 1-modified MMPs and probe 2-modified PMPs were mixed with MB155, and the mixture was loaded to the inlet. As the microchannel is hydrophilic after plasma treatment, this water-based solution would spontaneously flow towards the other end, driven by capillary force without the need for an external power source.

The mixture first passes the magnetic separator, which was designed as a human stomach-shape microchannel located next to the embedded permanent magnets (lower-left in Fig. 1 and Fig. S1†). The flow field was calculated based on CFD (Fig. S2a and b†). Importantly, using the stomach-shape microchannel, the flow first slows down due to the expanding microchannel, and the stream is directly guided toward the strongest region of magnetic force (Fig. S2c†), which maximizes the opportunity for capturing the MMPs–targets–PMPs. Later, after passing the region of strong magnetic field, the microchannel further expands, resulting in an even slower flow before leaving for the trapping channel to minimize the escaping of the MMPs–targets–PMPs aggregates (Movie S2†). As such, efficient capturing of MMPs–targets–PMPs was achieved (Movie S3†).

To visually quantify the free PMPs carried to the downstream, a bead trap was designed as a narrowing nozzle with a minimum width of 8  $\mu\text{m}$ , which can block the PMPs with a diameter of 15  $\mu\text{m}$  (Movie S4†). Importantly, the depth of the PMP trapping channel was designed to be 25  $\mu\text{m}$ , such that the PMPs can be accumulated as a monolayer to maximize the visible length of PMP accumulation (Movie S4†). As a result, a white bar of accumulated PMPs was visually seen in the trapping channel, and its length can be quantified using a dipstick-type ruler (Fig. 2). For the blank sample, only MMPs were captured in the magnetic separator (Movie S5†), and all PMPs suspended in solution kept flowing towards the trapping channel (Movie S6†), giving rise to the longest PMP accumulation. Comparatively, for the sample with the MB155 target, a portion of PMPs would be retained at the site of the magnetic separator, shortening the length of PMP accumulation.

During bead trapping, the water-based buffer solution can penetrate through the gap between the PMPs and the nozzle. Importantly, the capillary pump was placed after that to ensure the capillary attraction of liquid wicking until the

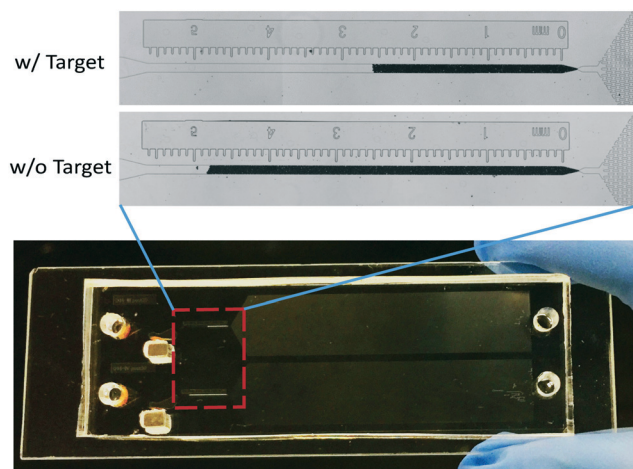


Fig. 2 Optical images showing the visual bar for a sample with the MB155 target (upper) and a blank sample (lower). In the presence of target oligonucleotides, the visual bar became shorter, providing a visual and quantitative readout.

capillary pump is fully filled (volume capacity: 4.07  $\mu\text{l}$ ), which ensures the consistent volume that fills the microchannel and minimizes the data fluctuation between each experiment.

### Limit of detection of oligonucleotides

We explored the limit of detection of oligonucleotides based on different amount of the MB155 target, *i.e.* 0 mol, 10 fmol, 20 fmol, 40 fmol, 60 fmol, 100 fmol, 200 fmol and 2000 fmol in 20  $\mu\text{l}$ . Fig. 3a illustrates the length of accumulated PMPs in the trapping channel at different amount of MB155 targets, which reflects the amount of free PMPs escaping from the magnetic separator. As expected, the PMP accumulation was inversely proportional to the target amount. For the blank sample (0 mol), most of the PMPs can escape from the magnetic separator and accumulate in the trapping channel, resulting in the longest white bar. In contrast, when the target amount increased, the trapping length decreased. According to the length of PMP accumulation with respect to the target amount (Fig. 3), the linear range of such a change is from 0 mol to 60 fmol (inset in Fig. 3b), and the limit of detection can be determined to be 13 fmol (0.65 nM in 20  $\mu\text{l}$ ,  $S/N = 3$ , calculated on the basis of  $3\sigma/k$ , where  $\sigma$  is the standard deviation of the blank sample, and  $k$  is the absolute slope of the linear equation,  $-0.0254$ ), demonstrating a performance comparable to that of UV/vis spectrometry.<sup>20</sup>

### Analysis of single-nucleotide polymorphisms

We next investigated the selectivity of detection in the microfluidic device using single-nucleotide polymorphisms (SNP). The selectivity is crucial for differentiating non-specific hybridization.<sup>30,31</sup> To test it, the seventh base of the MB155 target from the 5' end, G, was replaced by A, T and C, and de-

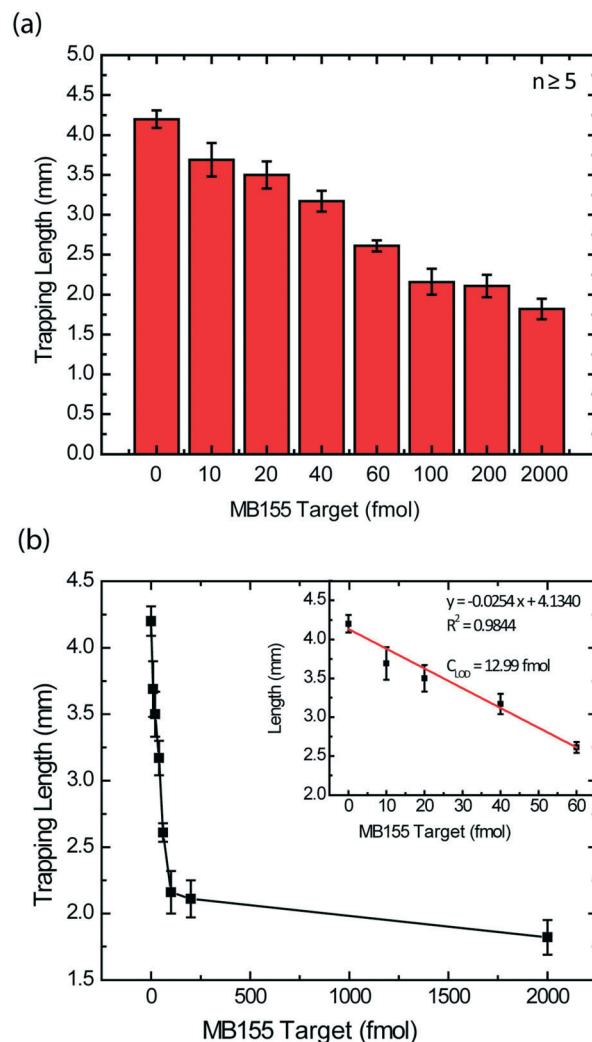
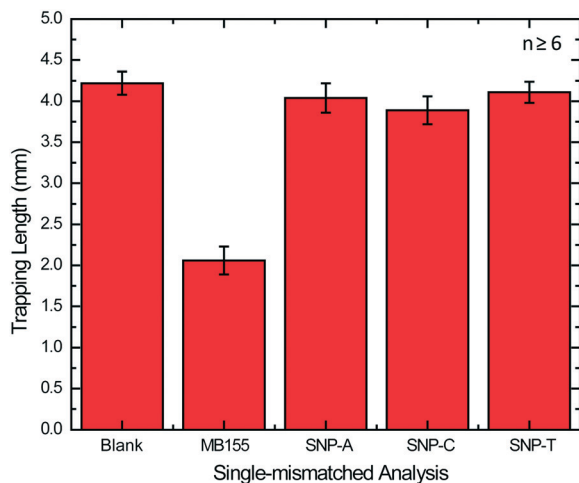


Fig. 3 Limit of detection of target oligonucleotides. (a) Length of accumulated PMPs in the trapping channel based on different amount of MB155 targets (mean  $\pm$  SEM,  $n \geq 5$ ). (b) The length of PMP accumulation with respect to the target amount showing a linear change between 0–60 fmol. Limit of detection was calculated from the linear regression in the inset (mean  $\pm$  SEM,  $n \geq 5$ ).

noted as SNP-A, SNP-T, and SNP-C, respectively. Using 200 fmol (10 nM in 20  $\mu\text{l}$ ) for each case, the length of PMP accumulation showed that the results of SNP-A, SNP-T and SNP-C almost had no difference with that of the blank sample (0 mol) (around 4.20 mm in length, Fig. 4). In contrast, for the MB155 target, the length was significantly shorter (2.00 mm). Thus, the result demonstrated that this microfluidic-based bead trap can provide a remarkable performance for differentiating single-nucleotide polymorphisms.

### Detection in a 10% v/v serum environment

In addition, we also explored the compatibility of our device in a complex bio-fluid. Blood serum contains proteins, cells, RNAs, and DNase/RNase, and such interfering materials may lead to considerable challenges for hybridization and even



**Fig. 4** Analysis of single-nucleotide polymorphisms. SNP-A, SNP-C and SNP-T are single-base mutated sequences of MB155, by using A, C and T to replace the seventh base G in MB155, respectively (mean  $\pm$  SEM,  $n \geq 6$ ).

cause failure of device functionality. To investigate the tolerance to such a complex environment, we used a 10% v/v serum environment containing varied amount of MB155 (0 fmol, 10 fmol, 20 fmol, 40 fmol, 60 fmol, 100 fmol, 200 fmol and 2000 fmol in 20  $\mu$ l), without any further pre-treatment. Similar to the results obtained in the buffer solution, the length of PMP accumulation decreased with an increase of the target amount (Fig. 5). While the overall length increased slightly because a small number of MMPs–targets–PMPs were carried to the bead trap due to the high viscosity of serum, the limit of detection is around 20 fmol, which demonstrated the compatibility with a complex bio-fluid and the ability to tolerate the interfering materials in such a microfluidic device.

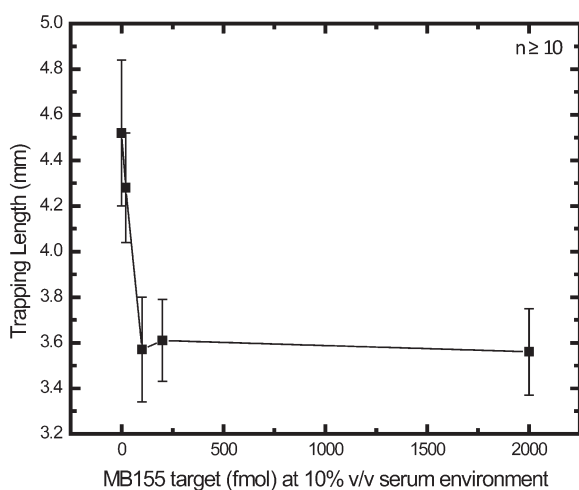


**Fig. 5** Detection in a 10% v/v serum environment (mean  $\pm$  SEM,  $n \geq 10$ ).

### Application to detection of lead ions

Based on the characterization above, we tested a model application that uses detection of oligonucleotides for monitoring lead ions (Fig. 6a). On the basis of nucleic acid hybridization, it was reported that DNAzyme, a form of DNA oligonucleotide, could catalyze a specific hydrolytic cleavage in the presence of lead ions.<sup>9–12</sup> Accordingly, we replaced the target oligonucleotide MB155 by GR-5 DNAzyme, which exhibits a high selectivity towards  $\text{Pb}^{2+}$ .<sup>9</sup> This DNAzyme consists of a substrate strand GRDS (blue in Fig. 6a) and an enzyme strand GRE (orange in Fig. 6a), and the two termini of GRDS were extended and designed to be able to hybridize with MB155 probe 1 and probe 2, respectively. As such, if  $\text{Pb}^{2+}$  is absent, the GR-5 DNAzyme at the amount of 200 fmol (10 nM

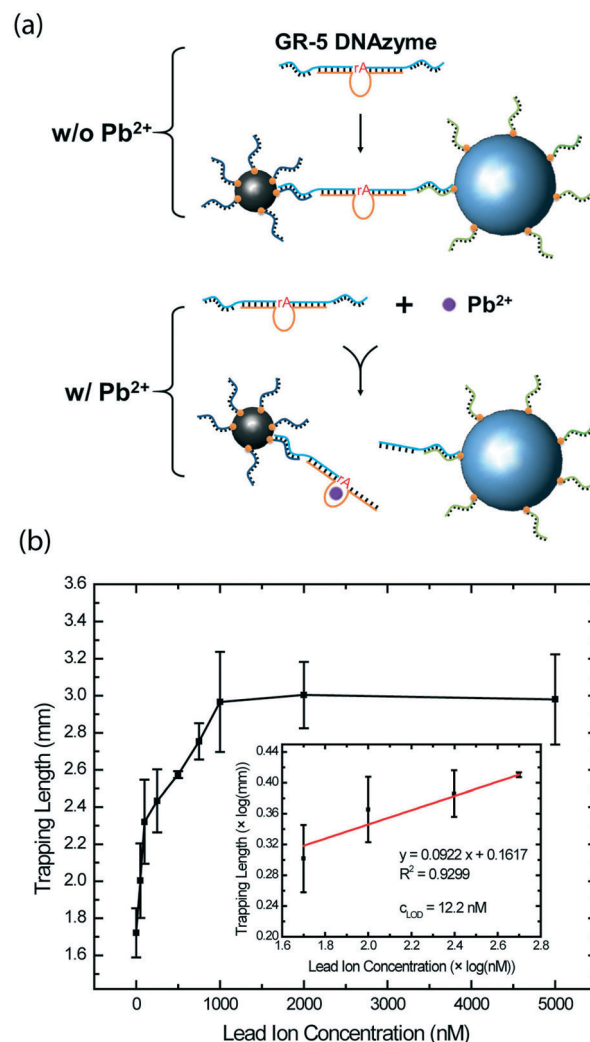


**Fig. 6** Application to detection of lead ions. (a) Schematics of the detection of lead ions based on the employment of GR-5 DNAzyme to connect MMPs and PMPs. When  $\text{Pb}^{2+}$  is present, it cleaves the GRDS substrate strand (blue) at the RNA site (rA), allowing more PMPs to accumulate at the trapping channel. (b) The length of PMP accumulation with respect to the concentration of lead ions, where the limit of detection was calculated from the linear regression in the inset (mean  $\pm$  SEM,  $n \geq 5$ ).

in 20  $\mu\text{l}$ ) can connect MMPs and PMPs, leading to the formation of a sandwiched structure, MMPs–DNAzyme–PMPs. In contrast, when  $\text{Pb}^{2+}$  is present, it cleaves the substrate strand at the RNA site (rA) into two parts through a phosphodiester bond cleavage, which prevents the formation of the sandwiched structure MMPs–DNAzyme–PMPs and allows more PMPs to accumulate in the trapping channel.

We tested different concentrations of  $\text{Pb}^{2+}$  solution, including 0 nM, 50 nM, 100 nM, 250 nM, 500 nM, 750 nM, 1000 nM, 2000 nM and 5000 nM. As expected, the trapping length due to PMP accumulation reflected the concentrations of  $\text{Pb}^{2+}$  with a positive proportion (Fig. 6b). Moreover, using the log scale, the linear range of such a change was from 0 to 250 nM (inset in Fig. 6b), and the limit of detection can be determined to be 12.2 nM ( $S/N = 3$ , calculated on the basis of  $3\sigma/k$ , where  $\sigma$  is the standard deviation of the blank sample, and  $k$  is the absolute slope of the linear equation, 0.0922). Remarkably, the limit of detection is below the maximum human exposure to drinking water, 48 nM ( $10 \mu\text{g l}^{-1}$ ), according to the guideline of the World Health Organization. As such, with sufficient sensitivity and the ease of intensive sample preparation when applied in drinking/clean water, our results demonstrated a feasible application for monitoring lead ion contamination.

## Conclusions

In this work, we demonstrate a microfluidic-based bead trap capable of forming a visual bar for quantitative detection of oligonucleotides. The MMPs and PMPs can be connected in the presence of the target molecules, forming MMPs–targets–PMPs. Driven by capillary force, the solution first passes the magnetic separator, in which the magnetophoretic effect removes the MMPs–targets–PMPs *via* an external magnetic field. With the use of a narrowing nozzle, free PMPs would be accumulated in the trapping channel, forming a visible bar with length inversely proportional to the amount of target oligonucleotides. This platform can differentiate single-mutated sequences and is compatible with a complex bio-fluid environment. Moreover, by using a  $\text{Pb}^{2+}$  dependent DNAzyme oligonucleotide, we demonstrate the detection of lead ions with a limit of detection lower than the standard of maximum human exposure, providing a simple, sensitive approach achieving visual detection and direct quantification of lead contamination on a power-free and instrumental-free platform.

## Conflicts of interest

There are no conflicts to declare.

## Acknowledgements

We acknowledge the support from the Early Career Scheme (project no. 21214815) and the General Research Fund (project no. 11277516 and 11217217) from the Hong Kong Research Grant Council, the Science Technology and Innovation Committee of Shenzhen Municipality (Grant No.

JCYJ20150601102053061 and JCYJ20170307091338607), and the internal grant from the City University of Hong Kong (Grant No. 6000537).

## Notes and references

- 1 M. Bezdicek, M. Lengerova, D. Ricna, B. Weinbergerova, I. Kocmanova, P. Volfova, L. Drgona, M. Poczova, J. Mayer and Z. Racil, *Med. Mycol.*, 2016, **54**, 714–724.
- 2 A. L. Greninger, S. N. Naccache, S. Federman, G. Yu, P. Mbala, V. Bres, D. Stryke, J. Bouquet, S. Somasekar, J. M. Linnen, R. Dodd, P. Mulembakani, B. S. Schneider, J. J. Muyembe-Tamfum, S. L. Stramer and C. Y. Chiu, *Genome Med.*, 2015, **7**, DOI: 10.1186/s13073-13015-10220-13079.
- 3 M. G. Campana, M. T. Hawkins, L. H. Henson, K. Stewardson, H. S. Young, L. R. Card, J. Lock, B. Agwanda, J. Brinkerhoff, H. D. Gaff, K. M. Helgen, J. E. Maldonado, W. J. McShea and R. C. Fleischer, *Mol. Ecol. Resour.*, 2016, **16**, 1224–1239.
- 4 I. Ziegler, A. Fagerström, K. Strålin and P. Mölling, *PLoS One*, 2016, **11**, e0167883.
- 5 G. Xu, R. N. Gunson, J. M. Cooper and J. Reboud, *Chem. Commun.*, 2015, **51**, 2589–2592.
- 6 T. Sato, A. Takayanagi, K. Nagao, N. Tomatsu, T. Fukui, M. Kawaguchi, J. Kudoh, M. Amagai, N. Yamamoto and N. Shimizu, *J. Clin. Microbiol.*, 2010, **48**, 2357–2364.
- 7 Q.-Y. Xie, Y.-H. Wu, Q.-R. Xiong, H.-Y. Xu, Y.-H. Xiong, K. Liu, Y. Jin and W.-H. Lai, *Biosens. Bioelectron.*, 2014, **54**, 262–265.
- 8 F. Wei, P. B. Lillehoj and C.-M. Ho, *Pediatr. Res.*, 2010, **67**, 458–468.
- 9 H.-B. Wang, L. Wang, K.-J. Huang, S.-P. Xu, H.-Q. Wang, L.-L. Wang and Y.-M. Liu, *New J. Chem.*, 2013, **37**, 2557–2563.
- 10 Y. Wang and J. Irudayaraj, *Chem. Commun.*, 2011, **47**, 4394–4396.
- 11 J. Liu and Y. Lu, *J. Am. Chem. Soc.*, 2003, **125**, 6642–6643.
- 12 Y. Huang, Y. Ma, Y. Chen, X. Wu, L. Fang, Z. Zhu and C. J. Yang, *Anal. Chem.*, 2014, **86**, 11434–11439.
- 13 J. Thavanathan, N. M. Huang and K. L. Thong, *Biosens. Bioelectron.*, 2014, **55**, 91–98.
- 14 S. C. Gopinath, T. Lakshmipriya and K. Awazu, *Biosens. Bioelectron.*, 2014, **51**, 115–123.
- 15 C. Ma, W. Wang, A. Mulchandani and C. Shi, *Anal. Biochem.*, 2014, **457**, 19–23.
- 16 X. Mao, Y. Ma, A. Zhang, L. Zhang, L. Zeng and G. Liu, *Anal. Chem.*, 2009, **81**, 1660–1668.
- 17 H. D. Hill and C. A. Mirkin, *Nat. Protoc.*, 2006, **1**, 324–336.
- 18 M. Liong, A. N. Hoang, J. Chung, N. Gural, C. B. Ford, C. Min, R. R. Shah, R. Ahmad, M. Fernandez-Suarez, S. M. Fortune, M. Toner, H. Lee and R. Weissleder, *Nat. Commun.*, 2013, **4**, 1752.
- 19 H. Zhou, J. Kim, F. Zou, K. Koh, J. Y. Park and J. Lee, *Sens. Actuators, B*, 2014, **198**, 77–81.
- 20 Z. Zhao, S. Chen, J. K. L. Ho, C.-C. Chieng and T.-H. Chen, *Analyst*, 2015, **140**, 7876–7885.

- 21 S. Chen, L. T. Chu, P. P. Yeung, Z. Zhao, Y. Bao, M. S. Chan, P. K. Lo and T.-H. Chen, *ACS Appl. Mater. Interfaces*, 2015, 7, 22821–22830.
- 22 R. Elghanian, J. J. Storhoff, R. C. Mucic, R. L. Letsinger and C. A. Mirkin, *Science*, 1997, 277, 1078–1081.
- 23 R. Kanjanawarut and X. Su, *Anal. Chem.*, 2009, 81, 6122–6129.
- 24 F. Xia, X. Zuo, R. Yang, Y. Xiao, D. Kang, A. Vallée-Bélisle, X. Gong, J. D. Yuen, B. B. Hsu, A. J. Heeger and K. W. Plaxco, *Proc. Natl. Acad. Sci. U. S. A.*, 2010, 107, 10837–10841.
- 25 A. Lesniewski, M. Los, M. Jonsson-Niedziółka, A. Krajewska, K. Szot, J. M. Los and J. Niedziółka-Jonsson, *Bioconjugate Chem.*, 2014, 25, 644–648.
- 26 J. S. Lee, M. S. Han and C. A. Mirkin, *Angew. Chem., Int. Ed.*, 2007, 46, 4093–4096.
- 27 M. Shellaiah, T. Simon, K. W. Sun and F.-H. Ko, *Sens. Actuators, B*, 2016, 226, 44–51.
- 28 Z. Li, Y. Wang, J. Wang, Z. Tang, J. G. Pounds and Y. Lin, *Anal. Chem.*, 2010, 82, 7008–7014.
- 29 Y. Liu, Z. Wu, G. Zhou, Z. He, X. Zhou, A. Shen and J. Hu, *Chem. Commun.*, 2012, 48, 3164–3166.
- 30 B. Dubertret, M. Calame and A. J. Libchaber, *Nat. Biotechnol.*, 2001, 19, 365–370.
- 31 E. M. Boon, D. M. Ceres, T. G. Drummond, M. G. Hill and J. K. Barton, *Nat. Biotechnol.*, 2000, 18, 1096–1100.